belt in the classical case (no planet migration). When the migration of giant planets is included or, more specifically, when the inward migration of Jupiter is included, those three resonances sweep through the region between 3.5 and 3.9 AU. Asteroids originally not in any resonances encounter those MMRs and get captured, and their orbits become chaotic (Fig. 3). It is this resonance-sweeping mechanism that depletes asteroids from the outer belt.

We also considered the effect of this mechanism on other parts of the asteroid belt. Asteroids outside 4 AU were removed, whereas asteroids were maintained in the 2:3 interior MMR at 3.97 AU (Fig. 2), consistent with the observed asteroid distribution. However, in our simulations, asteroids were captured and maintained in the 1:2 interior MMR at 3.28 AU, contrary to the observed gap at this location. A plausible explanation for this deficiency is the time scale of instability for asteroids in that resonance. In the classical case (no planet migration), the time scale to clear the 1:2 gap is on the order of 10 million years (*5*, *16*). A hint of this long-term effect is evident in Fig. 2E and is more obvious in Fig. 2B. We conclude that the asteroids at the 1:2 interior MMR were removed by the long-term perturbations of the planets after planet migration ceased (*17*).

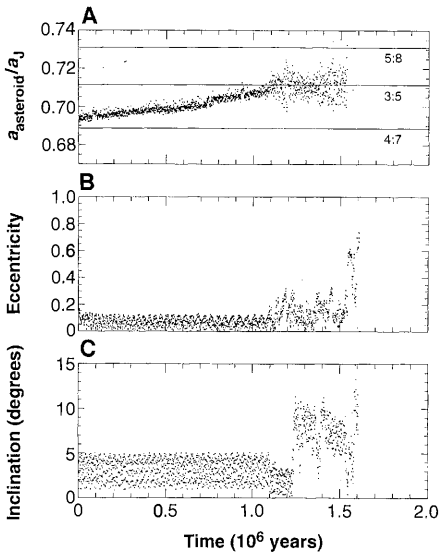

Fig. 3. Evolution of an asteroid in a sun-Jupiter-Saturn-asteroid system. The planetary migration time is 2 million years. (**A**) Semimajor axis of the test asteroid normalized to the semimajor axis of Jupiter. Three horizontal lines show the locations of the 5:8, 3:5, and 4:7 interior MMRs. As Jupiter migrated inward, the relative semimajor axis of the asteroid increased. This test asteroid was initially not in any MMR with Jupiter; however, the inward motion of Jupiter caused the 3:5 interior MMR to sweep by and capture this asteroid into resonance at 1.1 million years. The eccentricity (**B**) and inclination (**C**) of the asteroid varied irregularly when it was in resonance. Finally, its eccentricity increased to such an extent that it began to cross the orbit of Jupiter, and subsequent close encounters with the giant planet finally made its orbit hyperbolic and removed it from the outer belt.

REFERENCES AND NOTES

1. E. Bowell, *Asteroid Orbital Elements Database* (Lowell Observatory, Flagstaff, AZ, 1996).
2. S. F. Dermott and C. D. Murray, *Nature* **301**, 201 (1983). A MMR occurs when the orbital period of an asteroid is a simple multiple of Jupiter's orbital period. In addition to 1:2 and 2:3, interior MMRs are also associated with other gaps in the asteroid belt.
3. R. Greenberg and H. Scholl, in *Asteroids*, T. Gehrels, Ed. (Univ. of Arizona Press, Tucson, 1979), pp. 310–333; A. M. Nobili, in *Asteroids II*, R. P. Binzel, T. Gehrels, M. S. Matthews, Eds. (Univ. of Arizona Press, Tucson, 1989), pp. 862–879.
4. J. Wisdom, *Icarus* **72**, 241 (1987).
5. F. A. Franklin, *Astron. J.* **112**, 1247 (1996); A. Morbidelli, *ibid.* **111**, 2453 (1996).
6. B. Gladman and M. Duncan, *ibid.* **100**, 1680 (1990).
7. M. Lecar, F. Franklin, P. Soper, *Icarus* **96**, 234 (1992).
8. M. Duncan, in *Circumstellar Dust Disks and Planet Formation*, R. Ferlet and A. Vidal-Madjar, Eds. (Editions Frontieres, Gif-sur-Yvette, 1994), pp. 245–255.
9. R. Malhotra, *Nature* **365**, 819 (1993).
10. ———, *Astron. J.* **110**, 420 (1995).
11. J. A. Fernández and W.-H. Ip, *Icarus* **58**, 109 (1984); *Planet. Space Sci.* **44**, 431 (1996).
12. E. Everhart, in *Dynamics of Comets: Their Origin and Evolution*, A. Carusi and G. B. Valsecchi, Eds. (Reidel, Boston, 1985), pp. 185–202.
13. R. Malhotra, *Celestial Mech. Dyn. Astron.* **60**, 373 (1994).
14. Integration of a test asteroid was stopped, and the asteroid was presumed to have been removed from the population, if it came within 1 Hill radius r_H of a planet. Once an object is less than 1 r_H from a planet, the dominant perturber is the planet, not the sun. The Hill radii of Jupiter and Saturn are 0.36 and 0.44 AU, respectively.
15. M. J. Holman and N. W. Murray, *Astron. J.* **112**, 1278 (1996).
16. R. Malhotra, unpublished material.
17. Because of the geometric locations of the 4:7, 3:5, and 5:8 interior MMRs, Jupiter has to migrate inward, by about 0.2 AU, to remove asteroids in the 3.5- to 3.9-AU region. However, the migration time scale and the migration scheme (linear, exponential, or other) are less constrained on the basis of the population of asteroids in this region. The long-term dynamics of the asteroids at 2:3 and 1:2 interior MMRs after the planet migration ceased may provide more insight into these questions.

18. We thank H. Zook for enthusiastic discussions. This research was performed while J.-C.L. held a National Research Council–NASA Johnson Space Center Research Associateship and R.M. was a staff scientist at the Lunar and Planetary Institute (LPI), which is operated by the Universities Space Research Association under contract NASW-4574 with NASA. Support was also provided by NASA's Origins of Solar Systems Research Program under grant 4474. This paper is LPI contribution 905.

4 September 1996; accepted 15 November 1996

Kinetic Measurement of the Step Size of DNA Unwinding by *Escherichia coli* UvrD Helicase

Janid A. Ali and Timothy M. Lohman*

The kinetic mechanism by which the DNA repair helicase UvrD of *Escherichia coli* unwinds duplex DNA was examined with the use of a series of oligodeoxynucleotides with duplex regions ranging from 10 to 40 base pairs. Single-turnover unwinding experiments showed distinct lag phases that increased with duplex length because partially unwound DNA intermediate states are highly populated during unwinding. Analysis of these kinetics indicates that UvrD unwinds duplex DNA in discrete steps, with an average "step size" of 4 to 5 base pairs (approximately one-half turn of the DNA helix). This suggests an unwinding mechanism in which alternating subunits of the dimeric helicase interact directly with duplex DNA.

DNA helicases are motor proteins that function to unwind duplex (ds) DNA during DNA replication, recombination, and repair and are also components of eukaryotic transcription complexes (*1*, *2*). These enzymes use the chemical energy obtained from nucleoside triphosphate binding or hydrolysis (or both) to perform the mechanical work of unwinding dsDNA, which also requires translocation of the helicase along DNA for processive unwinding.

The *Escherichia coli* UvrD helicase [helicase II (*3*)] plays essential roles in both methyl-directed mismatch repair (*4*) and nucleotide excision repair of DNA (*5*), and in humans, defects in these processes are linked to increased susceptibility to cancer (*6*). UvrD protein [720 amino acids; molecular mass of 81,989 (*7*)] forms dimers in the absence of DNA (*8*), and the dimeric form of the enzyme is functional in DNA unwinding (*9*). In fact, the functional forms of most DNA helicases are oligomeric (mainly dimers or hexamers), most likely because multiple DNA binding sites are needed for helicase function (*1*, *10*, *11*). UvrD displays a 3′-to-5′ polarity in DNA unwinding (*12*), in that a 3′ single-stranded (ss) DNA flanking the duplex facilitates initiation of unwinding in vitro (*9*); however, UvrD can also initiate unwinding at a nick (*13*). UvrD shares about

Department of Biochemistry and Molecular Biophysics, Washington University School of Medicine, 660 South Euclid Avenue, Box 8231, St. Louis, MO 63110, USA.

*To whom correspondence should be addressed.

40% sequence similarity with the *E. coli* Rep protein (*14*), also a dimeric 3′-to-5′ DNA helicase (*15*, *16*), and can form heterodimers with Rep (*17*). Thus, the mechanisms of unwinding for these two helicases are likely to be similar. The dimeric Rep helicase appears to unwind dsDNA by an active, rolling mechanism (*16*), a central feature of which is that both subunits of the Rep dimer can bind either ss- or dsDNA, and a key intermediate is a complex in which both ss- and dsDNA are bound simultaneously to the dimer. A prediction of this model is that the helicase unwinds dsDNA in discrete steps and that multiple base pairs are unwound per step, that is, unwinding occurs with a "step size" (m) of >1 base pair (bp).

To estimate the step size for UvrD-catalyzed DNA unwinding, we performed single-turnover kinetics (with respect to DNA) with the DNA substrates listed in Table 1 (*18*) at 25°C in buffer U (*19*) using rapid quenched-flow techniques (*20*). Each DNA substrate (1 nM final concentration) was first incubated with excess UvrD protein, and the reaction was initiated by rapid mixing with adenosine triphosphate (ATP) (1.5 mM final concentration) and a large excess (5 μM final concentration) of $dT(pT)_{15}$ (where T is thymidylate); the latter serves to prevent reinitiation of unwinding by trapping free UvrD or UvrD that dissociates during unwinding (*20*). The amount of unwound DNA was determined for each time point by nondenaturing polyacrylamide gel electrophoresis (*20*). Unwinding of a 3′-$(dT)_{40}$-18 bp DNA (substrate II) catalyzed by UvrD [80 nM (monomers)] was rapid, with ~60% of the DNA molecules unwound within 0.5 s (Fig. 1). However, unwinding occurred with a distinct lag phase, which in a single-turnover experiment indicates the presence of at least one intermediate along the pathway to fully unwound DNA.

This lag phase is not due to reannealing of the fully unwound DNA because the half-life for reannealing is >2.5 hours at 1 nM DNA (*21*). It also does not reflect a slow protein-DNA binding step because the UvrD-DNA complexes were preformed before the addition of ATP and the rate of the lag phase is independent of UvrD concentration (*22*). Although DNA unwinding requires an oligomeric form of the UvrD protein [most likely a dimer (*9*)], the lag phase does not result from a linkage to protein assembly, because the excess $dT(pT)_{15}$ added with the ATP prevents binding of free UvrD to the DNA substrate. Time courses determined at lower concentrations of ATP (as low as 5 μM), where the unwinding rate becomes limited by ATP binding, also showed distinct lag phases (*9*). Therefore, the lag phase does not result from a fortuitous situation in which DNA unwinding is preceded by unrelated processes that have comparable rates because the lag phase would be eliminated by lowering the ATP concentration into a range such that unwinding is limited by the rate of ATP binding. Rather, this lag phase suggests that DNA unwinding occurs by a multistep process with highly populated intermediate states along the pathway to fully unwound DNA. The rate constants for the formation and decay of these intermediates must also be comparable in magnitude, otherwise a lag phase would not be observed (*23*).

One likely explanation for the lag phase is that partially unwound DNA molecules are formed as intermediates during unwinding. Even though the "all or none" assay used in these experiments cannot directly detect such partially unwound intermediate states, their presence would be detectable as a lag phase, if they are sufficiently populated. If this hypothesis is correct, then the magnitude of the lag phase should increase with the DNA duplex length. We therefore examined the unwinding kinetics of a series of DNA substrates varying in duplex length, L, with L = 10, 18, 24, and 40 bp (substrates I through IV, respectively, in Table 1). A lag phase was observed with each DNA substrate, and the lag phase increased with duplex length (Fig. 2A).

We analyzed the time courses in Fig. 2A to determine the number of "steps" required by UvrD to unwind each duplex and thus the number of base pairs unwound in each step, that is, the unwinding step size, m. The simplest mechanism that yields a lag phase for unwinding is the sequential n-step mechanism outlined in Scheme 1, where preformed productive UvrD-DNA complexes, $(U\text{-}DNA)_L$, form the partially unwound DNA intermediates, $I_{(L-m)}$, $I_{(L-2m)}$, $I_{(L-3m)}$, and so on along the pathway to fully unwound ssDNA, where the subscripts refer to the number of base pairs remaining in the duplex.

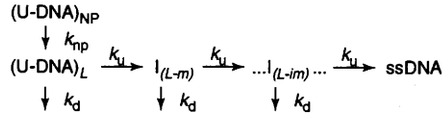

Scheme 1

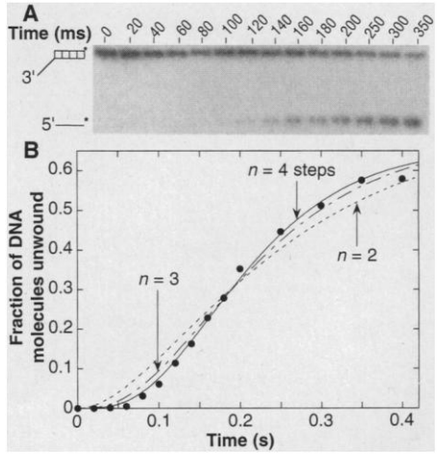

Fig. 1. Single-turnover kinetic time course for UvrD-catalyzed unwinding of a 3′-$(dT)_{40}$-18 bp duplex shows a distinct lag phase. Experiments were performed with 80 nM UvrD (monomer concentration) and 1 nM DNA substrate II (Table 1) at 25°C in buffer U (*19*). Reactions were initiated by the addition of 1.5 mM ATP and 5 μM $dT(pT)_{15}$ and quenched by Na_3EDTA (*20*). (**A**) Image of a 20% nondenaturing polyacrylamide gel after electrophoresis of the ^{32}P end-labeled DNA obtained from the rapid quench experiments. The time after addition of ATP is indicated for each lane. (**B**) Unwinding time course plotted as the fraction of duplex molecules unwound. The lines are simulations based on the nonlinear least squares fits (*27*) to Eq. 1 with n = 2 (k_{obs} = 7.8 ± 1.2 s^{-1}, xA_L = 0.70 ± 0.79), n = 3 (k_{obs} = 12.9 ± 1 s^{-1}, xA_L = 0.67 ± 0.08), or n = 4 (k_{obs} = 18.4 ± 1 s^{-1}, xA_L = 0.64 ± 0.07).

Table 1. DNA unwinding substrates.

Substrate	Structure	Sequence of top strand of duplex
I	3′-(T_{40})-10-5′	5′-GCCTCGCTGC-3′
II	3′-(T_{40})-18-5′	5′-GCCTCGCTGCCGTCGCCA-3′
III	3′-(T_{40})-24-5′	5′-GCCCTGCTGCCGACCAACGAAGGT-3′
IV	3′-(T_{40})-40-5′	5′ GCCCTGCTGCCGACCAACGATGGTTACATTCCCGCTGCTG-3′
V	3′-(T_{40})-18-5′	5′-GGGCGGGCCAATAAATAA-3′

In our analysis we have assumed that the net unwinding rate constants, k_u, are equivalent for each step because the lag will be largest when all the rate constants are equal (*23*, *24*). Although each k_u may depend on base composition or sequence (or both), this assumption seems justified (*24*). Scheme 1 also assumes that UvrD can dissociate with rate constant k_d at each step in the unwinding reaction. In that these experiments were performed at saturating ATP concentrations, we have not explicitly included any steps associated with ATP binding, hydrolysis, or release of adenosine diphosphate (ADP) and inorganic phosphate. Hence, k_u and k_d are macroscopic rate constants with contributions from nucleotide binding and release.

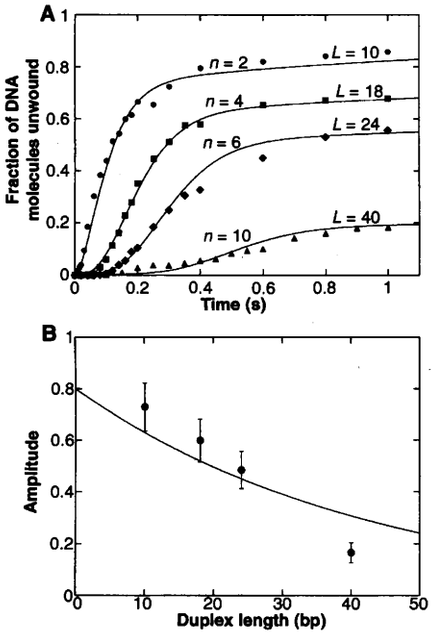

Fig. 2. The effect of dsDNA length on the single-turnover kinetics of UvrD-catalyzed DNA unwinding. UvrD (80 nM) was incubated with 1 nM DNA: (●) substrate I (L = 10), (■) substrate II (L = 18), (◆) substrate III (L = 24), and (▲) substrate IV (L = 40), and unwinding was initiated with 1.5 mM ATP and 5 μM $dT(pT)_{15}$ (*20*). (**A**) Data from all four time courses were globally fitted (*27*) to Scheme 1 with Eq. 1 by fixing n = 2, 4, 6, and 10 for the L = 10-, 18-, 24-, and 40-bp substrates, respectively. The fitted values of k_{obs}, k_{NP}, and x were constrained to be the same for each time course, whereas the amplitude for each time course was floated. The best fit parameters are as follows: L = 10 bp (n = 2, A_L = 0.911 ± 0.034); L = 18 bp (n = 4, A_L = 0.75 ± 0.032); L = 24 bp (n = 6, A_L = 0.605 ± 0.031); and L = 40 bp (n = 10, A_L = 0.215 ± 0.03), with k_{obs} = 18.6 ± 1.3 s^{-1}, k_{NP} = 0.76 ± 0.06 s^{-1}, and x = 0.8 ± 0.07 (average step size $m = L/n$ = 4.4 bp). (**B**) Amplitudes of the lag phase, $A_1 = xA_L$, as a function of duplex length, L. The smooth curve is the nonlinear least squares fit of the data to $A_1 = xP^{L/m}$, constraining m = 4.4. The processivity per step is P = 0.9 ± 0.07. (See text for a full explanation of the variables.)

Scheme 1 also incorporates the fact that some fraction of the DNA is bound to UvrD in nonproductive complexes, $(U\text{-}DNA)_{NP}$, which must slowly isomerize with rate constant k_{NP} to form productive complexes before the DNA can be unwound (*25*).

On the basis of Scheme 1, the expression for the fraction of DNA molecules unwound as a function of time, $F(t)$, is given in Eq. 1, where $k_{obs} = k_u + k_d$, n is the number of steps in the unwinding reaction, x is the fraction of DNA molecules bound to UvrD in complexes that are productive for DNA unwinding, A_L is the total amplitude of the unwinding reaction, and k_{NP} is a macroscopic rate constant for conversion of nonproductive to productive UvrD-DNA complexes (*26*).

$$F(t) = A_L\left[x\left\{1 - \sum_{r=1}^{n}\frac{(k_{obs}\,t)^{r-1}}{(r-1)!}e^{-k_{obs}t}\right\} + (1-x)(1-e^{-k_{NP}t})\right] \quad (1)$$

Figure 1B shows the nonlinear least squares fits of Eq. 1 to the unwinding time course for the 18-bp duplex (substrate II) obtained by constraining n to values of 2, 3, or 4 steps (*27*). It is clear that n = 4 provides a better fit than either n = 2 or 3. However, because of the existence of the second slow unwinding phase, analysis of a single time course only provides a minimum estimate of the number of steps and thus a maximum estimate of the step size (L/n) (*28*). Therefore, from analysis of this single experiment, we can only conclude that there are at least three intermediates in the pathway to fully unwind an 18-bp duplex and thus the step size $m \leq$ ~4.5 bp.

Simultaneous fitting to Eq. 1 of all four time courses in Fig. 2A for the DNA substrates varying in duplex length, L, does provide additional constraints to obtain upper limits on n (*28*). A consistent set of n values (*28*, *29*) was chosen for the four duplexes, and we performed a nonlinear least squares global fit using all four time courses to obtain the best estimates of k_{obs}, k_{NP}, x, and A_L (Fig. 2A). The smooth curves in Fig. 2A were simulated by using Eq. 1 and the best fit parameters for each substrate (see legend to Fig. 2). As expected, the number of steps, n, increases with duplex length, L, with the best fit (integer) values of n determined to be 2, 4, 6, and 10 for L = 10-, 18-, 24-, and 40-bp duplexes, respectively. For all four DNA substrates, the unwinding step size, m, determined from the ratio L/n varied from 4.0 to 5.0 bp, with an average value of 4.4 bp. Therefore, UvrD unwinds about one-half turn of a B-form DNA duplex in each step. The fact that all time courses in Fig. 2A are well described by the same value of k_{obs} = 18.6 ± 1.3 s^{-1} for the observed per step unwinding rate, independent of duplex length, provides further support for the proposed mechanism.

Figure 2A also shows that the fraction of DNA molecules unwound decreases with increasing duplex length. These experiments were performed in the presence of excess $dT(pT)_{15}$ that prevents reinitiation of unwinding by dissociated UvrD; therefore this observation indicates that the fraction of UvrD dissociating during unwinding increases with duplex length. Thus, DNA unwinding by UvrD is not highly processive under these conditions. The processivity of unwinding per step, defined as $P = k_u/(k_u + k_d)$ or equivalently as $P = (N-1)/N$, where N is the average number of steps taken before dissociation (*1*), is the probability of unwinding the next m base pairs. A low processivity results in some fraction of the DNA molecules not being unwound because of dissociation of the helicase before the DNA is fully unwound. The amplitudes of the lag phase (A_1) as a function of L are plotted in Fig. 2B. On the basis of the mechanism in Scheme 1, A_1 is equal to $xP^{L/m}$, where x is the initial fraction

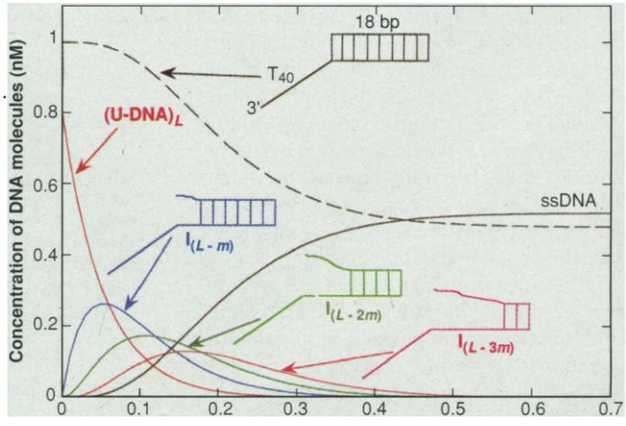

Fig. 3. Simulated kinetic profile for unwinding of an 18-bp duplex showing the transient formation of partially unwound intermediates. Simulations were performed with KINSIM (*32*), Scheme 1, and the best fit kinetic parameters for UvrD unwinding of DNA substrate II (18 bp) (n = 4, k_u = 16.7 s^{-1}, k_d = 1.9 s^{-1}, x = 0.8). Unwinding proceeds by means of three partially unwound DNA intermediates, resulting in a lag phase for production of fully unwound ssDNA. Upon quenching or dissociation of UvrD, partially unwound intermediates reanneal to reform fully dsDNA.

of bound productive complex. The best fit of the data in Fig. 2B to this function yields $P = 0.9 \pm 0.07$ per step (*29*). Therefore UvrD takes an average of $N = 10$ steps before dissociating. In that $k_{obs} = 18.6 \pm 1.3\ s^{-1}$, we calculate $k_u = 16.7 \pm 0.1\ s^{-1}$ and $k_d = 1.9 \pm 1.2\ s^{-1}$, although we emphasize that these do not represent the rate constants for the elementary steps of unwinding and dissociation.

The predicted time courses of the partially unwound DNA intermediates and fully unwound ssDNA for an 18-bp duplex, based on Scheme 1 and the best fit kinetic parameters, is shown in Fig. 3. Both the decay of fully duplex molecules and the formation of fully unwound ssDNA occurs with a lag phase. Note also that the final amplitude of unwinding is not equal to the initial amount of productively bound duplex $(U\text{-}DNA)_L$, reflecting the low unwinding processivity of the UvrD helicase, that is, during the unwinding process, UvrD can dissociate from the DNA with some finite probability. Once dissociated from the UvrD, any partially unwound DNA intermediate will reanneal to reform the original duplex. Such reannealing must occur even for a partially unwound 10-bp substrate, which goes through only one intermediate. If this intermediate did not reanneal upon dissociation of the helicase, but rather proceeded forward to complete unwinding, then a lag phase would not be observed for the 10-bp substrate.

Previous studies of the *E. coli* Rep helicase, which functions as a dimer, have led to the proposal that DNA unwinding occurs by an "active, rolling" mechanism in which the two subunits of the dimer alternate in binding dsDNA, while the other subunit remains bound to the 3′ ssDNA region (*16*). Upon ATP hydrolysis, a region of the dsDNA, containing m base pairs (where $m > 1$) is unwound and the 5′ ssDNA displaced while the Rep subunit remains bound to the 3′ strand. Release of the 3′ ssDNA from the other subunit then enables the unwinding cycle to continue (*16*, *30*). Our finding that UvrD helicase unwinds dsDNA in steps of about one-half turn of the duplex is consistent with this mechanism. These results indicate that a rate-limiting step during unwinding occurs every ~5 bp. A step size of 5 bp would be observed provided that the rate of unwinding the 5 bp is much faster than the next (rate-limiting) step. This rate-limiting step might reflect translocation of one UvrD subunit to the duplex region ahead of the fork, rather than the actual unwinding event.

The unwinding step size of ~4 to 5 bp that we have determined for UvrD represents the average number of base pairs unwound per successful unwinding cycle. It does not likely represent the number of base pairs unwound per ATP hydrolyzed, although the efficiency with which ATP hydrolysis is coupled to DNA unwinding remains to be measured. However, on the basis of studies of the *E. coli* Rep helicase (*11*), it seems likely that this coupling efficiency is low because in a rolling model one subunit of the helicase is always bound to the ssDNA and this subunit is able to continually hydrolyze ATP.

REFERENCES AND NOTES

1. T. M. Lohman and K. P. Bjornson, *Annu. Rev. Biochem.* **65**, 169 (1996).
2. S. W. Matson, D. W. Bean, J. W. George, *BioEssays* **16**, 13 (1994).
3. V. F. Maples and S. R. Kushner, *Proc. Natl. Acad. Sci. U.S.A.* **79**, 5616 (1982).
4. R. S. Lahue, K. G. Au, P. Modrich, *Science* **245**, 160 (1989).
5. P. R. Caron, S. R. Kushner, L. Grossman, *Proc. Natl. Acad. Sci. U.S.A.* **82**, 4925 (1985); I. Husain, B. van Houten, D. C. Thomas, M. Abdel-Monem, A. Sancar, *ibid.*, p. 6774.
6. A. Sancar, *Science* **266**, 1954 (1994); P. Modrich, *ibid.*, p. 1959.
7. Y. Yamamoto *et al.*, *J. Biochem.* **99**, 1579 (1986).
8. G. T. Runyon, I. Wong, T. M. Lohman, *Biochemistry* **32**, 602 (1993).
9. J. Ali and T. M. Lohman, in preparation.
10. T. M. Lohman, *Mol. Microbiol.* **6**, 5 (1992); *J. Biol. Chem.* **268**, 2269 (1993).
11. K. P. Bjornson, I. Wong, T. M. Lohman, *J. Mol. Biol.* **263**, 411 (1996).
12. S. W. Matson, *J. Biol. Chem.* **261**, 10169 (1986).
13. G. T. Runyon and T. M. Lohman, *ibid.* **264**, 17502 (1989); G. T. Runyon, D. G. Bear, T. M. Lohman, *Proc. Natl. Acad. Sci. U.S.A.* **87**, 6383 (1990).
14. C. A. Gilchrist and D. T. Denhardt, *Nucleic Acids Res.* **15**, 465 (1987).
15. K. Chao and T. M. Lohman, *J. Mol. Biol.* **221**, 1165 (1991).
16. I. Wong and T. M. Lohman, *Science* **256**, 350 (1992).
17. I. Wong, M. Amaratunga, T. M. Lohman, *J. Biol. Chem.* **268**, 20386 (1993).
18. UvrD protein was purified and its concentration determined spectrophotometrically (*8*). Oligodeoxynucleotides were synthesized and purified, and dsDNA substrates (5′ end-labeled on the top strand with ^{32}P) were prepared as described (*31*). DNA substrates had a $(dT)_{40}$ ssDNA attached to the 3′ end of the bottom strand. Oligodeoxythymidylates were used to avoid intramolecular base pairing within the ssDNA. A 40-nucleotide 3′ ssDNA is optimal for the initiation of DNA unwinding by UvrD in vitro, and a 5′ ssDNA tail does not facilitate initiation of DNA unwinding (*9*).
19. Buffer U is 25 mM tris-HCl, pH 7.5, 6 mM NaCl, 2.5 mM $MgCl_2$, 5 mM 2-mercaptoethanol, 10% (v/v) glycerol, and 0.1 mg/ml bovine serum albumin (BSA). Buffer A is 25 mM tris, pH 7.5, at 25°C, 6 mM NaCl, 5 mM 2-mercaptoethanol, and 10% (v/v) glycerol.
20. Kinetics experiments were performed (25°C, buffer U) with a three-syringe, quenched-flow apparatus (KinTek RQF-3, University Park, PA). UvrD at twice the final concentration was premixed with DNA substrate (2 nM) in buffer A plus 2 mM $MgCl_2$ and BSA (0.2 mg/ml), incubated on ice for 20 min, and then loaded in one loop (45 μl) of the quench flow. The other loop (45 μl) contained ATP (twice the final concentration) in buffer A plus 3 mM $MgCl_2$ and 10 μM $dT(pT)_{15}$. Samples were incubated for 3 min at 25°C (incubation times of 6 min did not affect the reaction). Reactions were initiated by rapidly mixing the two solutions, yielding buffer U, and quenched after times from 2 ms to 100 s by the addition of 0.4 M Na_3EDTA in 10% (v/v) glycerol. The fraction of ssDNA at time $t = 0$ was determined by mixing the UvrD-DNA solution with buffer A plus 3 mM $MgCl_2$ (without ATP). Quenched samples were analyzed by nondenaturing 20% polyacrylamide gel electrophoresis to separate ds- from ssDNA. Quenching with Na_3EDTA also caused dissociation of UvrD from the DNA, so that the DNA was deproteinated before electrophoresis. Radioactivity in each band was quantitated with a Betascope 603 blot analyzer (Betagen, Waltham, MA), and the fraction of DNA duplexes unwound at each time was calculated as described (*30*). The low DNA substrate concentration (1 nM) prevented reannealing of fully unwound DNA. The amplitude and rate of the lag phase were independent of the $dT(pT)_{15}$ concentration (0 to 25 μM).
21. K. P. Bjornson, M. Amaratunga, K. J. M. Moore, T. M. Lohman, *Biochemistry* **33**, 14306 (1994).
22. Single-turnover unwinding rates (measured with DNA substrates I and II) were independent of the UvrD concentration [3 nM to 150 nM (monomer)]; hence, unwinding initiates from prebound complexes. The apparent equilibrium dissociation constant for UvrD binding to the substrate is 1 to 2 nM; hence, at 80 nM UvrD, all the DNA is bound to UvrD.
23. H. Gutfreund, *Kinetics for the Life Sciences. Receptors, Transmitters and Catalysts* (Cambridge Univ. Press, Cambridge, England, 1995).
24. This assumption is reasonable because each DNA substrate has a similar base composition (high G+C content), and the time courses with different length duplexes can be globally fitted to Eq. 1 with the same k_{obs} and step size. Also, experiments with two 18-bp substrates (II and V in Table 1) differing in A+T content both fit to mechanisms with $n = 4$ steps with similar k_{obs}. Global analysis of simulated time courses also showed that the step size determination was not influenced when the unwinding rate constants of alternate steps differed by twofold, although k_{obs} was affected.
25. Even in the presence of a high concentration of $dT(pT)_{15}$, a second slower unwinding phase with a small amplitude remains, which represents unwinding by UvrD bound in a nonproductive form that must first isomerize with rate constant k_{NP} to form a productive complex.
26. The first term in Eq. 1 is the fraction of DNA molecules unwound by the productive $(U\text{-}DNA)_L$ complexes (*23*), where $x = (U\text{-}DNA)_L/[(U\text{-}DNA)_L + (U\text{-}DNA)_{NP})]$; thus $xA_L = A_1$ is the amplitude of the lag phase. The second term in Eq. 1, with amplitude $(1 - x)A_L$, reflects slower unwinding by nonproductive complexes (*25*).
27. Nonlinear least squares analyses were performed with Scientist (MicroMath Scientific Software, Salt Lake City, UT) and plotted with KaleidaGraph (Synergy Software, Reading, PA). Uncertainties are reported as 95% confidence limits.
28. Because of the second slow phase (*25*), analysis of a single time course provides only a minimum estimate of the number of steps, n. Equally good fits are obtained for greater values of n by decreasing the amplitude and increasing the rate of the lag phase, respectively, because these changes can be compensated by increases in both the amplitude and the value of k_{NP} for the slow phase. However, simultaneous analysis of all four time courses in Fig. 2A (floating each value of A_L) and globally fitting for the same values of x, k_{obs}, and k_{NP} provides additional constraints on the upper limit of n for each duplex, assuming the step size, $m = L/n$, is independent of L. Global fits with $m = 2$ or 3 gave poorer fits.
29. Analysis of data in Fig. 2B assumed a constant average step size of $m = L/n = 4.4$, and that the amplitudes, A_1, are a smooth function of duplex length; however, A_1 may decrease in a step-wise manner with L, and this may contribute to our non-integer (4.4) estimate of the step size.
30. M. Amaratunga and T. M. Lohman, *Biochemistry* **32**, 6815 (1993).
31. I. Wong, K. L. Chao, W. Bujalowski, T. M. Lohman, *J. Biol. Chem.* **267**, 7596 (1992).
32. B. A. Barshop, R. F. Wrenn, C. Frieden, *Anal. Biochem.* **130**, 134 (1983).

33. We thank I. Wong, K. Bjornson, and K. Moore for critical discussions; M. Amaratunga for preliminary experiments; W. van Zante and T. Ho for DNA synthesis; and P. Burgers, R. Gregorian, and J. Hsieh for comments on the manuscript. Supported in part by NIH grant GM45948.

1 July 1996; accepted 25 November 1996